QUALITY OF THE 3D POINT CLOUD OF A TIME-OF-FLIGHT CAMERA UNDER LUNAR SURFACE ILLUMINATION CONDITIONS: IMPACT AND IMPROVEMENT TECHNIQUES

Kentaro Uno[1], Louis-Jerome Burtz[2], Masafumi Endo[1], Kenji Nagaoka[1], Kazuya Yoshida[1]

[1] *Tohoku University, Aoba 6-6-01, Aramaki, Aoba-ku, Sendai, Japan,*
E-mail: {unoken, nagaoka, yoshida}@astro.mech.tohoku.ac.jp, masafumi.endo.s2@dc.tohoku.ac.jp
[2] *ispace, inc., Azabudai 3-1-6, Iikura katamachi, Minato-ku, Tokyo, Japan, E-mail: l-burtz@ispace-inc.com*

ABSTRACT

Time-of-Flight (ToF) cameras can deliver dense 3D point clouds by precisely calculating the round-trip time of infrared (IR) light reflecting off objects. A Japanese Lunar exploration rover employs a commercial off-the-shelf ToF camera as its main hazard-detection sensor. The lighting conditions on the Moon reduce the quality of the three-dimensional (3D) point cloud. In this paper, we explore the effects of the Lunar surface lighting conditions on the range, validity, and accuracy of the data delivered by the ToF camera. To achieve repeatable results, an indoor Lunar lighting testbed was developed. Based on these experiments, we propose a filtering method to fuse the 3D point cloud frames obtained at different integration times.

1 INTRODUCTION

In recent years, as a popular alternative to stereoscopic cameras, time-of-flight (ToF) cameras have attracted attention for applications in space robot awareness systems. A recent example is the Astrobee project [2], a robot scheduled to be launched this year to work alongside the astronauts in the International Space Station (ISS). It monitors its environment and avoid hazards assisted by a ToF camera. ToF cameras can deliver dense three-dimensional (3D) point clouds by accurately calculating the round-trip time of the infrared (IR) light reflected off objects. Considering their particular application on the surface of the Moon, ToF cameras have certain advantages:

- They are effective in sensing unstructured, featureless surfaces such as the Lunar surface.
- As they rely on active illumination, they can obtain a 3D point cloud regardless of shadows.
- Compared to rotating LiDARs, they have no moving parts which allows them to resist the rocket launch environment.
- Their mass, power consumption, volume, and computing complexity are compatible with the miniaturized architecture of a microrover.

SORATO, the Japanese Lunar exploration rover managed by ispace, inc. shown in Figure 1, employs a Sentis3D–M100 commercial off-the-shelf ToF camera, manufactured by the BECOM Bluetechnix Inc. as its main hazard-detection sensor. We previously experimentally demonstrated that the selected ToF camera hardware is suitable for space missions to the Lunar surface, through comprehensive qualification tests [3].

This paper is based on the prior work performed to characterize noise and errors of the 3D point cloud of the ToF camera. In particular, they showed the dependency of the optical characteristics (such as reflectivity) on the surface of the target object [5]. To correct for the variance in the data, a number of effective filtering methods were reported in [4] to acquire smoothed point clouds. However, most of the related studies are performed in indoor environments. This paper focuses on the characteristics of the extreme lighting conditions of the Lunar surface.

The paper begins with a presentation of the characteristics of the Lunar surface lighting conditions and the hardware improvements to the ToF camera to achieve a maximum resilience to extreme sunlight conditions. In Chapter 3, we present an optical testbed, developed to perform repeatable experiments with the camera hardware under conditions matching those of the Lunar surface. We demonstrate the effect on the quality of the 3D point cloud for the respective integration times at distances of 1 m and 2 m. Based on the results and analysis, in Chapter 4 we propose a software filtering method consisting in the fusion of several 3D point clouds obtained at key integration times. We discuss the impact on the three quality metrics: achievable range, validity, and accuracy. In the last part of the paper we apply these techniques to an experiment conducted in a Lunar-analog facility in JAXA.

Figure 1 : Flight model of Japanese Lunar exploration microrover © HAKUTO/ispace. A visible light camera is fitted on the front (top round lens) and it uses a ToF camera as the hazard detection sensor (middle round lens for the receiver and golden IR window for the laser emitter).

Figure 2 : Intense sunlight on the surface of the Moon generates critical negative effects on both standard cameras (Apollo image above © NASA) and ToF cameras.

2 IMPACT OF SUNLIGHT ON THE TOF CAMERA SENSOR

2.1 Optical Conditions on the Lunar Surface

On the surface of the Moon, the absence of atmosphere allows the higher intensity sunlight to reach the surface. The solar spectral irradiance data measured by orbital spacecrafts are freely available, while the "Standard Solar Constant and Zero Air Mass Solar Spectral Irradiance Tables", defined by the ASTM International Standard E490-00a list the spectral irradiance values in the range of 120–1000 nm [6]. In the range of 840–860 nm, the irradiance is 2.0 mW/cm^2. The reason for the integration range of 840–860 nm is the effective sensitivity of the ToF camera sensor, discussed in the next subsection.

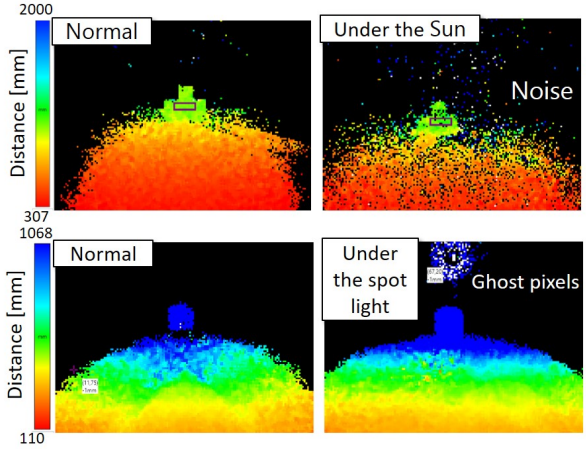

Figure 3 : Comparison of distances between the cloudy (left) and strong sunlight (right) conditions as well as between the ambient (top) and strong spot light (bottom) conditions.

2.2 Effect on the ToF Camera Sensor

We observed two main types of negative effects in the 3D point clouds obtained under strong sunlight illumination conditions. The images in Figure 3 show the raw data acquired by the ToF camera in two configurations (the distance value is color-coded according to the scale and the unit is mm). On the left pane, the optical environment is moderate (outdoor but cloudy) while on the right pane, the optical environment is challenging.

The first type of noise is general ambient noise (shown on the top of Figure 3). We believe that this phenomenon occurs when the external IR flux saturates the sensitive pixels, even while using the patented suppression of background illumination method[1]. The pixel circuit cannot perform correct phase calculations and outputs unrealistic distance values. We observed that the drop in signal-to-noise ratio (SNR) affects the entire frame.

The second type of noise is shown on the bottom of Figure 3. In this case, a well defined circular pattern can be observed on the upper part of the image. However, no such object was physically present in the scene. We interpret this signal as a strong collimated light reflected in the lens assembly, which selectively saturated the pixels in the shown circular region. This type of noise is known as ghost pixels. We previously presented additional discussion and more details on these specific mechanisms [3].

The aim of this paper is to explore the strategies to suppress these two types of noises, first through hardware improvements and then through software methods.

2.3 Hardware Improvements against the Sunlight

From a hardware point of view, the spectral sensitivity of the sensor of our ToF camera (PMD PhotonICs 19k-S3)

is in the range of 650–1200 nm. Its spectral sensitivity is particularly high in the range of 800–900 nm. However, the useful signal from the ToF camera emitter is only ~850 nm. The noise from the external sunlight is strong all over the visible and IR bands.

To maximize the SNR, a 20 nm band-pass filter was implemented together with the manufacturer. This filter is custom made and it has the smallest possible bandwidth, considering the central wavelength accuracy of the vertical-cavity surface-emitting laser (VCSEL) emitters, the temperature variations between the emitters and the filter, and the field of view of the sensor (chief ray angle).

3 LUNAR SUNLIGHT DEMONSTRATION EXPERIMENT

This section presents the 3D point cloud capturing experiment under lighting conditions representative of the Lunar surface. First, we describe the capabilities of the equipment we developed. Then, we explain the experimental setup and its components. Third, we present and discuss the experimental results.

3.1 Irradiance Measurement Instrumentation

We developed a measurement device that has the same sensitivity as the ToF camera by using the same bandpass filter (840–860 nm). An overview of the device is shown in Figure 4. The sensing part consists of the OP950 photodiode, produced by the TT Electronics/Optek Technology, Inc. The connected CPU board can measure the voltage of the photodiode circuit.

In order to determine the irradiance from the measured voltage, we performed a calibration test. For this work, we used a Glacier X TE Cooled CCD Spectrometer spectral analyzer, manufactured by B&W Tek, Inc. For the reference light source, we used the SOLAX series XC–500EF artificial sunlight simulator, manufactured by SERIC, Inc. In this test, the voltage of the photodiode and the spectral irradiance were measured together. Throughout this test, we obtained the curve of the calibrated irradiance as a function of voltage, as shown in Figure 5. In the experiments of the following sections the irradiance monitoring was strictly performed with this calibrated irradiance sensor.

3.2 IR Emitter

To recreate the IR illumination conditions on the surface of the Moon, we developed an IR illumination simulator, shown in Figure 6. The system has seven powerful infrared emitter modules. A 850-nm dual junction infrared LED emitter (LZ4-00R608 manufactured by LED Engin Inc.) was chosen. The illumination was concentrated by a narrow field of view (half-angle at 50% from the maximum intensity of 7.4°) lens (LLC69N, manufactured by

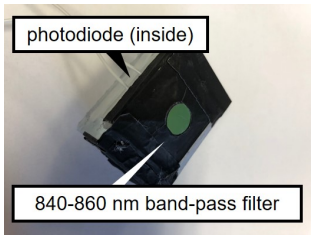

Figure 4 : Overview of the developed photodiode measurement system.

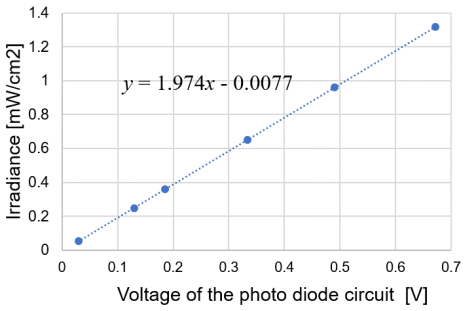

Figure 5 : Calibration curve obtained to determine the irradiance from the voltage of the photodiode circuit.

GAGGIONE Inc). A microcontroller controls their emission rate and monitors their behavior from a personal computer. The power sources are supplied directly from a 100 V household outlet.

The main features of the developed illumination simulator are:

- The sunlight simulator accurately represents the IR irradiance of the Sun for the wavelengths around 850 nm.
- It provides repeatable experiments opportunities (which is not possible with natural sunlight in outdoor environments).
- The modular concept of the IR emitter and lens allows for rapid prototyping of various illumination conditions.

The limitations of the setup as it was used in this study are:

- The illuminated area is small (however, suitable for the typical size of the hazards we are interested in imaging with the ToF camera).
- The irradiance received by the illuminated area is inversely proportional to the square of the distance to the emitters, which makes it highly variable and needs to be monitored with the developed irradiance logger.

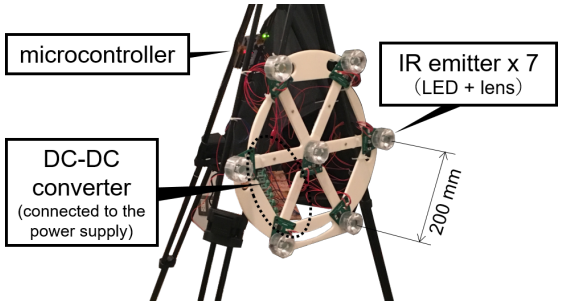

Figure 6 : IR illumination simulator consisting of 7 IR emitting modules.

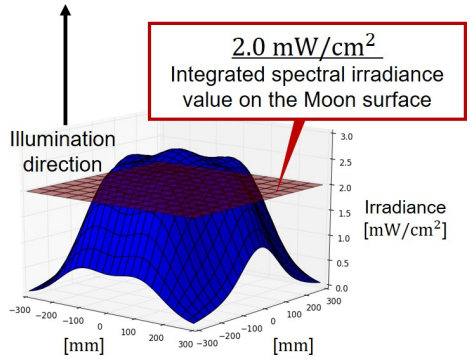

Figure 7 : Simulation of the 840–860 nm irradiance output for the 7-emitter configuration based on measurements of a single IR emitter module.

- To ensure reliability and repeatability, the IR emitters can be turned on for 1 s long flashes only, and then 10 s are needed to cool down. This requires synchronization with the ToF camera for data acquisition.

3.3 Experimental Conditions

Figure 8 shows an overview of the experimental environment. In the experiments, a checkerboard made of white squares (surface of normal printing paper) and black squares (printed by black ink), which have different IR reflectivities, were set on the wall as target objects. The checkerboard is fully illuminated by the developed IR emitters. The illumination condition on the checkerboard was measured (Figure 9). To stay above the 2.0 mW/cm^2 threshold, we defined the region-of-interest (ROI) as the central four squares in the checkerboard. The ToF camera was set in such a way to enable the acquisition of the center position of the target and the real world distance data was recorded. Moreover, using the irradiance measurement instrumentation, we verified that the ambient room illumination had no measurable IR component and therefore no effect on the ToF camera.

In this experiment, a 3D point cloud together with the change of integration time in the range of 100–2500 μs at every 100 μs were produced by the ToF camera. And

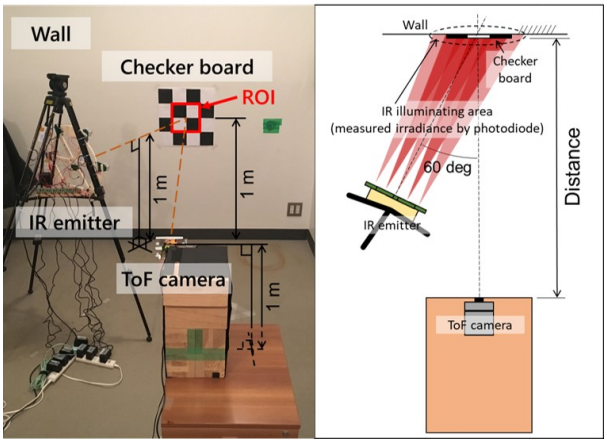

Figure 8 : Experimental setup. The ToF camera takes a 3D point cloud of the checkerboard illuminated by the IR emitters. The illumination condition is measured by the irradiance detector developed.

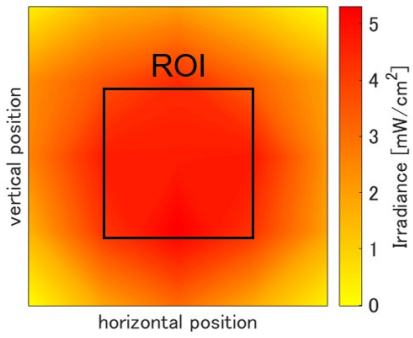

Figure 9 : Verification of the Illumination condition on the checkerboard. The yellow–red color shows the change in irradiance. The region-of-interest (ROI) has higher than Lunar surface irradiance.

this test was performed for the cases where the real-world distances were 1 m and 2 m. For each pixel of each point cloud, we set two amplitude-based thresholds to define the under/over-exposure of the pixels. The lower threshold is 300 and the higher one is 15000 (amplitude values are dimensionless, 2 byte integers). When the amplitude value is under or over the thresholds, the distance value of the pixel becomes −1 and 0 respectively.

3.4 Experimental Result and Discussion

Using the controlled environment presented earlier, we quantify the impact of the Lunar lighting conditions on the quality of the 3D point cloud with three metrics: range, validity and accuracy. At 1m, the ROI corresponds to 289 pixels on the ToF camera sensor. At 2m, the ROI corresponds to 64 pixels.

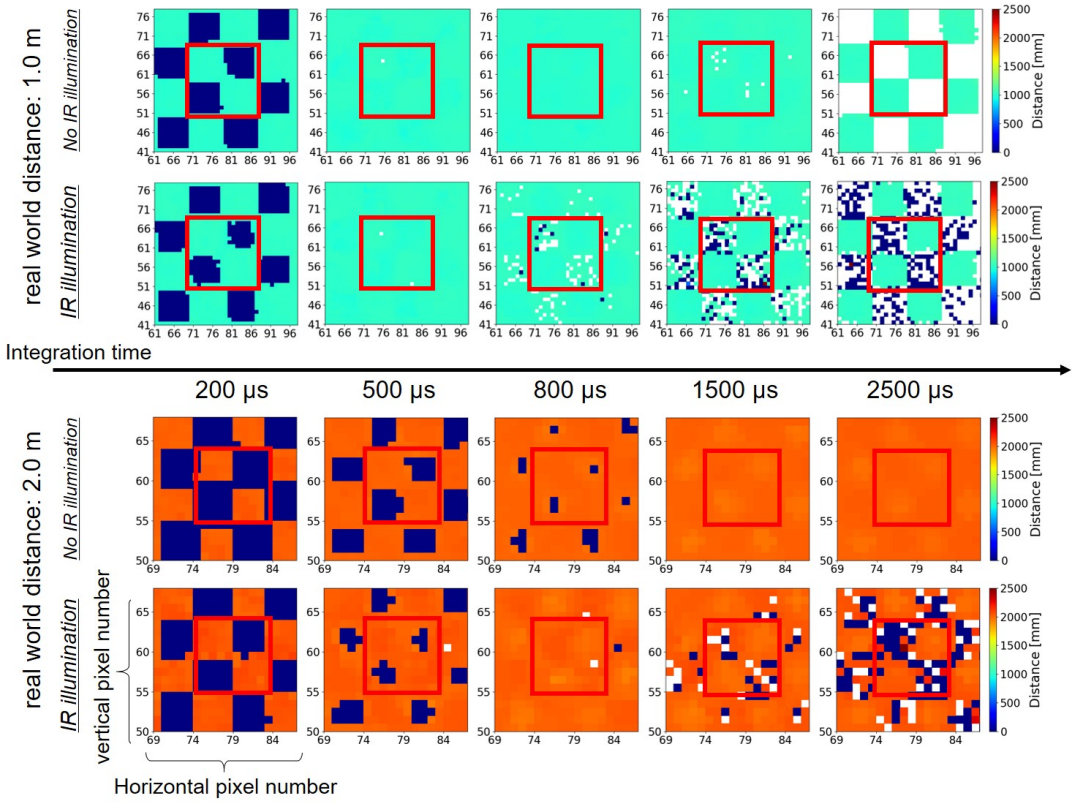

Figure 10 : Colorized distance maps of the checker board target (with ROI in the center, shown as a red square). Integration time increases from left to right. The top set is 1 m real-world distance, the bottom set is 2 m. In each set, the top maps are with no external IR illumination, the bottom maps show the effect of external IR illumination. In each distance map, over exposure pixels are marked white and under exposure pixels are marked dark blue.

3.4.1 Range

Figure 10 arranges the experimental results according to integration time (increasing from left to right), real-world distance (top set is 1 m, bottom set is 2 m) and the impact of Lunar surface illumination conditions (no external IR for the first line of each set, Lunar surface equivalent external IR for the second line of each set). Figure 10 shows that the range metric is greatly impacted by the integration time, the external IR illumination and the reflectivity of the target. The range versus integration time trade-off can be summarized as follows: high integration times ($> 800\,\mu$s) allow the ToF camera to detect low IR reflectivity targets, even at further distances. However, once Lunar surface illumination conditions are applied, higher integration times also increase the amount of noise entering the sensor and therefore the amount of noisy pixels.

Those result show that the ToF camera's ability to obtain data from farther away (which is a key metric for Hazard Detection and Avoidance) is limited if we set only one integration time. The optimal integration time for low reflectivity (white checkerboard squares) and high reflectivity (black checkerboard squares) targets is different. Furthermore, the optimal integration time for 1 m and 2 m distances is also different.

3.4.2 Validity

As presented in section 3.3 the validity is defined based on the amplitude value of each pixel. The top lines of each set of maps of Figure 10 show that even without external IR illumination, some pixels are still valid. Underexposure pixels (dark blue) are present at low integration times. Overexposure pixels (white) are present at high integration times. To isolate the negative effect due only to the external IR illumination, we checked 10 frames obtained without IR illumination. If the pixel was invalid more than 7 times, we regarded it as invalid regardless of the effect of Lunar surface lighting conditions. Figure 11 shows the change of the number of under- and over-exposure pixels caused by the external IR illumination in the ROI according to the increase in the integration time. The top graph shows the effects that are not due to external IR illumination. We define three zones of interest. In zone (1), there is a significant and decreasing amount of under exposure. We interpret that it is purely because of the lack of sensitivity to detect the necessary modulated

IR signal of the ToF camera lasers. In zone (2), there is no under or overexposure. In zone (3), at 1 m distance, the number of over exposure pixels increases and reaches a constant value. This is due to all the high reflectivity pixels saturating due to the laser light of the ToF camera.

Next we consider the specific effects of Lunar surface lighting conditions. We identify the invalid pixels and subtract those that were already invalid even without the external IR illumination. This process creates the bottom plot of Figure 11. In zone (1), there are no new invalid pixels. This shows that the external IR illumination does not affect short integration times. In zone (2), the percentage of invalid pixels increases linearly with the integration time. In zone (3) the percentage of invalid pixels continues to increase linearly, except for the case of 1 m distance where the pixels where already saturated by the laser of the ToF camera itself (zone (3) in top graph of Figure 11).

We interpret the observation of both under- and overexposure pixels as due to the saturation of the sensitive pixels. When the imager combines the modulated light and the external light, it can lead to the saturation of the sensor: overexposure pixels are reported. When the imager is saturated by the external IR flux and cannot detect the modulated IR signal of the ToF camera itself: under exposure pixels are reported. In conclusion, the external IR illumination causes the validity metric of the quality of the 3D point cloud to deteriorate linearly once the integration time increases above the 500 us threshold.

3.4.3 Accuracy

We define the accuracy of the valid pixels dataset as the measure of their standard deviation (STD) and median offset. The offset is calculated as the difference between the real-world distance and the median value from the valid pixels. Figure 12 and Figure 13 show the change of the STD and offset of the distance value in ROI according to the change of the integration time. We can see that external IR made both standard deviation and the maximum offset worse. Still, both are still less than 3% of the real-world distance. This shows that the thresholding performed for determining the validity of the pixels in the previous subsection, is robust to the Lunar surface illumination conditions.

4 TECHNIQUES FOR IMPROVEMENT OF THE 3D POINT CLOUD

Based on these insights, we propose a filtering method to optimize the available range, validity and accuracy by fusing several 3D point cloud frames obtained by the variation of the integration time of the ToF camera. In related works, Oggier et al. developed an algorithm to automatically select the best integration time [7], and Kazmi et al. proposed a method to combine two frames captured

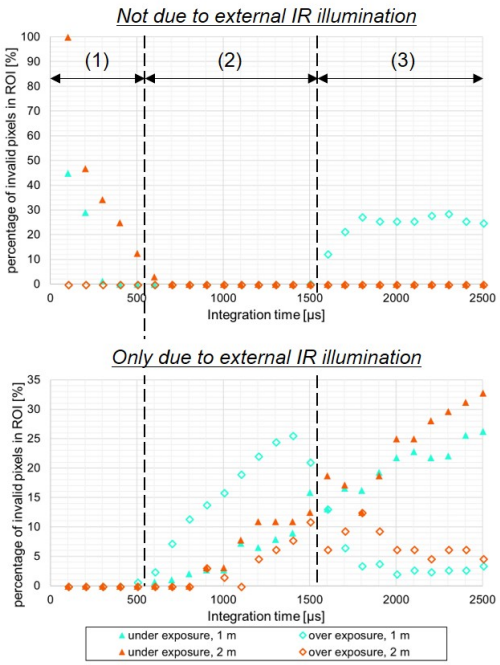

Figure 11 : The change of the percentage of under- and over- exposure pixels in ROI for each distance (1 m and 2 m). Top graph shows the pixels that are invalid regardless of the IR flux illumination. Bottom graph shows the pixels that are invalid only due to the effect external IR illumination.

at low and high integration times to increase the accuracy for short range objects [8]. For our application, 2 m range is required for the hazard detection algorithm of the rover. As discussed earlier, there is a trade-off between the long integration time resulting in an increased range, but also a higher sensitivity to sunlight noise.

4.1 Techniques and Performance

The following steps show the skeleton of the fusion algorithm:

1. Set the number and values of the integration time to be fused and capture the raw 3D point clouds.

2. Set the amplitude thresholds to define validity (under- and over- exposure). In each frame, identify the invalid pixels and remove them from further computation.

3. Compute the fused 3D point cloud: for each pixel, calculate the median of the amplitudes and distances based on the values from the frames captured at the different integration times. For each pixel, if there is no valid data from the raw point clouds at the various

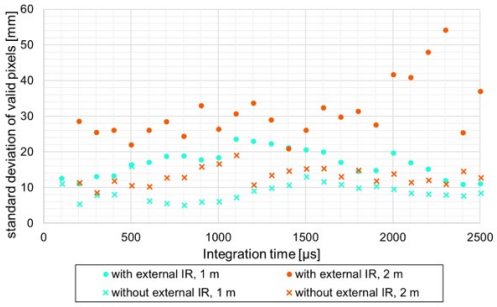

Figure 12 : Variation of the STD as a function of integration time for a target in the distance of 1 m away (in blue) and 2 m away (in orange).

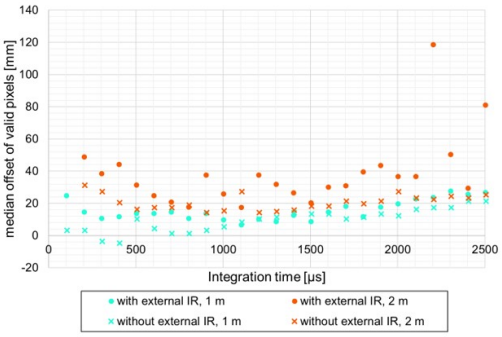

Figure 13 : Variation of the median offset from the ground truth (target 1 m away in blue and 2 m away in orange) as a function of integration time.

integration times selected, mark the pixel as invalid in the fused 3D point cloud also.

First, we applied this technique to the 3D point cloud dataset obtained in the experiment conducted in our laboratory (explained in Chapter 3). To keep the representativity with the Lunar rover implementation that has real-time computation and memory constraints, we fused only four frames. The integration times chosen are: 200, 600, 1000, and 1500 μs. Table 1 compares the quality metrics: validity (overexposure and underexposure), accuracy (standard deviation and offset) and range (minimum and maximum) for each frame and for the resulting fused frame. The bold font is attributed to the best result for each metric.

4.2 Implementation in a Lunar Analog Environment

Next, we applied our technique in an experiment performed in the advanced facility for space exploration of the Japan Aerospace Exploration Agency/Institute of Space and Astronautical Science (JAXA/ISAS) Sagamihara campus. In this test, the ToF camera located on the front side of the rover testbed detected three types of hazards: boulder, slope and ditches as defined in [3]. Figure 14 shows an overview of the slope hazard test. Artificial sunlight illuminated the entire test environment. The hazards themselves were additionally illuminated with the developed IR emitters (creating a 15cm diameter disk at the intensity of the Lunar surface lighting conditions). Using the same four integration times and the same technique as presented above, we obtained the 3D point clouds of Figure 15.

Figure 14 : Overview of the hazard slope test at the Sagamihara campus of JAXA.

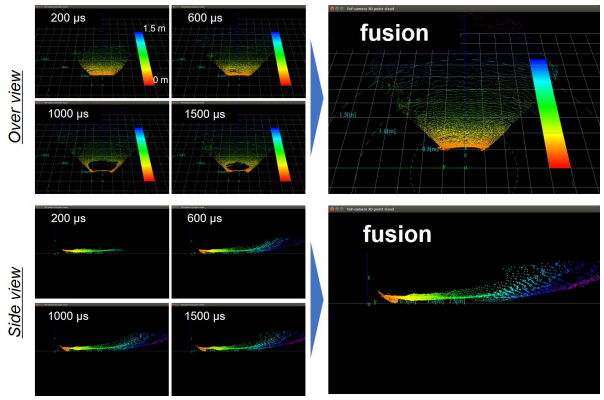

Figure 15 : 3D point cloud visualization of the raw frames at the four source integration times (left) and the output fused frame (right). View from the above (top) and view from the right hand side (bottom)

When the integration time is low (200 μs), the available range is narrow and short. Meanwhile, when the integration time is high (1000 μs and 1500 μs), the range increases and the slope is visible, but a significant area of invalid (overexposure) pixels can be observed at short range. However, regarding the fused frame (right two images in Figure 15), the quality is preserved at both short and long range. Through the result in Table 1 and Figure 15, we observe that the fusion method is able to combine almost all the best metrics of each individual frame. For the standard deviation, the best one is the frame at 1500 μs. This shows the necessary trade-off between the number of valid pixels and the standard deviation metric.

Table 1 : Comparisons of quality metrics: number of under/over-exposure pixels, offset, standard deviation, minimum range and maximum range. Bold font is attributed to the best result for each metric.

integration time [μs]	valid pixels in ROI [%]		underexposure in ROI [%]		over exposure in ROI [%]		standard deviation [mm]		median offset [mm]		range [mm]	
	(1 m)	(2 m)	(1 m)	(2 m)	(1 m)	(2 m)	(1 m)	(2 m)	(1 m)	(2 m)	(min)	(max)
200	70.9	53.1	29.1	46.9	**0**	**0**	15	52	**11**	29	**0.2**	1.2
600	96.9	96.9	0.7	3.1	2.4	**0**	14	30	18	26	**0.2**	1.6
1000	81.3	95.3	2.8	3.1	15.9	1.6	10	26	19	27	0.4	2.0
1500	62.6	76.6	15.9	12.5	21.5	10.9	**9**	**19**	21	26	0.5	**2.2**
fusion	**100**	**100**	**0**	**0**	**0**	**0**	14	27	14	**24**	**0.2**	**2.2**

5 CONCLUSION

This paper presents three main developments:

- We developed a Lunar surface lighting condition system to conduct repeatable experiments and an irradiance measurement tool to detect the energy received by the ToF camera sensor.
- We quantified the impact of extreme lighting conditions on the Lunar surface and their evolution with increasing integration times
- We implemented a software solution including the fusion of 3D point clouds taken at key integration times

The study on the impacts showed that several of the quality trade-offs are a function of the integration time. A longer integration time results in a higher amount of overexposure at short range, but also a higher number of valid points at long range. A shorter integration time also provides a higher SNR even under extreme sunlight illumination. The accuracy offset and STD vary with the integration time and there is a trade-off between a better STD value and a higher number of valid pixels.

In conclusion, we demonstrated that the ToF camera is able to capture 3D point cloud data accurately in challenging lighting conditions by the proposed improvement technique. The additional software processing, which fuses frames captured at various integration times, increases the quality of the data under high sunlight conditions such as those on the Lunar surface. As a result, this increases the suitability of the ToF camera to be a key component of the environment awareness system of an exploration robot.

Acknowledgement

We express our special thanks to BECOM Bluetechnix GmBH for their expertise and support, to KONICA MINOLTA for the irradiance measurement calibration and to JAXA/ISAS for the opportunity at their Lunar analog facility.

References

[1] T. Möller, H. Kraft, et al. (2005) "Robust 3D Measurement with PMD Sensors", In Proceedings of the 1st Range Imaging Research Day at ETH, Zurich, Switzerland.

[2] T. Smith, J. Bualat, et al. (2016), "ASTROBEE: A New Platform for Free-Flying Robotics on the International Space Station", *NASA Technical Reports Server*, ARC-E-DAA-TN31584.

[3] K. Uno, L-J. Burtz, et al. (2017), "Qualification of a Time-of-Flight Camera as a Hazard Detection and Avoidance Sensor for a Moon Exploration Microrover", *Transactions of The Japan Society for Aeronautical and Space Sciences, Aerospace Technology Japan*, in press.

[4] Y. Cui, S. Schuon, et al. (2010), "3D Shape Scanning with a Time-of-Flight Camera", In Proceedings of 2010 IEEE Conference on Computer Vision and Pattern Recognition (CVPR), San Francisco, USA, pp. 1173–1180.

[5] D. Falie, V. Buzuloiu. (2007), "Noise Characteristics of 3D Time-of-Flight Cameras", In Proceedings of the International Symposium on Signals, Circuits and Systems (ISSCS), Iasi, Romania.

[6] ASTM International. (2014), *Standard Solar Constant and Zero Air Mass Solar Spectral Irradiance Tables, Active Standard ASTM E490*, ASTM E490-00a, ASTM International, USA, pp. 2–13.

[7] T. Oggier, B. Bernhard, et al. (2005), "Swissranger sr3000 and first experiences based on miniaturized 3D-TOF cameras", In Proceedings of the 1st Range Imaging Research Day at ETH, Zurich, Switzerland.

[8] W. Kazmi, S. Foix, et al. (2012), "Plant Leaf Imaging using Time of Flight Camera under Sunlight, Shadow and Room Conditions", In Proceedings of the International Symposium on Robotic and Sensors Environments (ROSE). IEEE, Magdeburg, Germany pp. 192–197.